

PAPER • OPEN ACCESS

Development of optimised tissue-equivalent materials for proton therapy

To cite this article: H Cook et al 2023 Phys. Med. Biol. 68 075009

View the <u>article online</u> for updates and enhancements.

You may also like

- Tests of tissue equivalence for negative
- D F Jackson and K O'Leary
- <u>Stopping powers of a tissue-equivalent</u> gas for 40-200 keV protons A Fukuda
- Construction of a self-supporting tissueequivalent dividing wall and operational characteristics of a coaxial doublecylindrical tissue-equivalent proportional

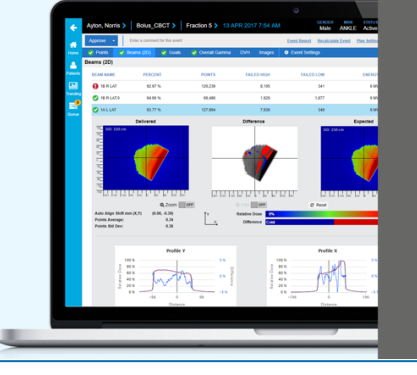
E A Saion and D E Watt



Powering Quality Management in Radiation Therapy

See why 1,600+ users have chosen SunCHECK for automated, integrated Patient QA and Machine QA.

Learn more >



Demo **SunCHECK**

Booth # 150



Physics in Medicine & Biology





OPEN ACCESS

RECEIVED

30 September 2022

REVISED

16 January 2023

ACCEPTED FOR PUBLICATION

25 January 2023

PUBLISHED

23 March 2023

Original content from this work may be used under the terms of the Creative Commons Attribution 4.0 licence.

Any further distribution of this work must maintain attribution to the author(s) and the title of the work, journal citation and DOL



PAPER

Development of optimised tissue-equivalent materials for proton therapy

H Cook^{1,2}, M Simard^{1,3,4}, N Niemann⁵, C Gillies⁶, M Osborne⁷, M Hussein^{1,2}, V Rompokos⁶, H Bouchard^{3,4}, G Royle¹, J Pettingell⁷, H Palmans^{2,8} and A Lourenço^{1,2}

- Department of Medical Physics and Biomedical Engineering, University College London, WC1E 6BT, United Kingdom
- ² Medical Radiation Science, National Physical Laboratory, Teddington, TW11 0LW, United Kingdom
- ³ Centre de recherche du CHUM, 900 Saint Denis St, Montreal, Quebec H2X 0A9, Canada
- ⁴ University of Montreal, 2900 Edouard Montpetit Blvd, Montreal, Quebec H3T 1J4, Canada
- ⁵ Barts Health NHS Trust, Clinical Physics Department, London, E1 2BL, United Kingdom
- ⁶ Medical Physics Department, Proton Therapy Centre, University College Hospital, WC1E 6AS, United Kingdom
- Medical Physics Department, The Rutherford Cancer Centre Thames Valley, Reading, RG2 9LH, United Kingdom
- 8 Medical Physics Group, MedAustron Ion Therapy Centre, A-2700 Wiener Neustadt, Austria

E-mail: hannah.cook@npl.co.uk

Keywords: Proton therapy, Phantoms, Tissue-equivalence

Abstract

Objective. In proton therapy there is a need for proton optimised tissue-equivalent materials as existing phantom materials can produce large uncertainties in the determination of absorbed dose and range measurements. The aim of this work is to develop and characterise optimised tissue-equivalent materials for proton therapy. Approach. A mathematical model was developed to enable the formulation of epoxy-resin based tissue-equivalent materials that are optimised for all relevant interactions of protons with matter, as well as photon interactions, which play a role in the acquisition of CT numbers. This model developed formulations for vertebra bone- and skeletal muscle-equivalent plastic materials. The tissue equivalence of these new materials and commercial bone- and muscleequivalent plastic materials were theoretical compared against biological tissue compositions. The new materials were manufactured and characterised by their mass density, relative stopping power (RSP) measurements, and CT scans to evaluate their tissue-equivalence. *Main results*. Results showed that existing tissue-equivalent materials can produce large uncertainties in proton therapy dosimetry. In particular commercial bone materials showed to have a relative difference up to 8% for range. On the contrary, the best optimised formulations were shown to mimic their target human tissues within 1%–2% for the mass density and RSP. Furthermore, their CT-predicted RSP agreed within 1%–2% of the experimental RSP, confirming their suitability as clinical phantom materials. Significance. We have developed a tool for the formulation of tissue-equivalent materials optimised for proton dosimetry. Our model has enabled the development of proton optimised tissue-equivalent materials which perform better than existing tissue-equivalent materials. These new materials will enable the advancement of clinical proton phantoms for accurate proton dosimetry.

1. Introduction

Tissue-equivalent phantoms are a vital tool for planning and dosimetric verification in end-to-end radiotherapy audits (Clark *et al* 2015, Thomas *et al* 2017, Carlino *et al* 2018, Taylor *et al* 2022). Phantoms are typically defined as a body of material that interacts with a type of radiation in the same manner as a patient (ICRU 1993). Over the past 50 years, a variety of phantoms have been developed for radiation modalities such as x-ray and electron treatments (Stacey *et al* 1961, Griffith *et al* 1976, White *et al* 1977, White 1978). In recent years, the number of proton therapy centres within the UK and worldwide has vastly increased (Crellin 2018). As a consequence, several studies (Palmans *et al* 2002, Al-Sulaiti *et al* 2012, Grant *et al* 2014, Lourenço *et al* 2017) have been

investigating the performance of existing phantom materials in proton beams. However, due to differences in radiation interaction with matter between photon and proton beams (Andreo $et\,al\,2017$, Paganetti 2017), phantom materials previously used for x-ray phantoms (White 1974) are not optimised, or sometimes unsuitable, for proton therapy.

Current phantom materials have been developed to mimic electron density and Hounsfield Unit (HU) for imaging and x-ray treatments (White 1974). However, for suitable phantom materials aimed at proton therapy, HU, relative stopping power (RSP), relative scattering power and nuclear interaction quantities should be mimicked as closely as possible. For reference dosimetry, which is recommended to be performed in water, the IAEA TRS-398 (Andreo et al 2000) states that plastic phantom materials should not be used due to the lack of information regarding water to plastic fluence corrections. Uncertainties caused by the tissue-equivalence of phantom materials have been also highlighted by Farr et al (2021) for the commissioning of intensity-modulated proton therapy system. Proton phantom development work by the Imaging and Radiation Oncology Core (IROC) group (Grant et al 2014, Branco et al 2017, Lewis et al 2018) emphasises the importance of a careful selection in phantom materials to ensure the phantom is adapted for proton dosimetry. Grant et al (2014) showed the need for phantom materials that are optimised for proton therapy, as only 50% of materials selected passed the 5% uncertainty criteria for correctly assigning stopping powers. In particular, bone materials were shown to produce large uncertainties for proton measurements. Goma et al (2018) showed that bone-equivalent materials, used in the stoichiometric calibration process, could result in an additional 3.5% uncertainty in RSP which could also be considered as additional range uncertainty. This is emphasised in the work by Lewis et al (2018) which showed that certain commercial bone-equivalent materials could cause up to 35% error in proton range.

Historically, most phantom material studies were reported by White (1974) and Constantinou (1978), who developed solid and gel-based tissue-equivalent materials for x-ray, electron beams and particle therapy (neutrons and protons). For proton therapy dedicated substitute materials, only mass density and mass stopping power were used within their model (Constantinou 1978). The new formulations were tested in a collimated scattered proton beam and the proton range as well as lateral profiles of the formulated materials compared to real tissue samples. Since then, most development of tissue-equivalent material has become a commercial activity. However, many tissue-equivalent materials are still based on the work of White (White 1974, Leeds Test Objects 2014). Water-equivalent materials for proton dosimetry were explored by Lourenço *et al* (2017) who assessed the particle fluence in commercial plastics against new plastic formulations. Their work highlighted a possible avenue of improvement of current tissue-equivalent materials for proton therapy by formulating new water-equivalent plastics which matched water within 1% for low- and high-energy proton beams in terms of particle fluence. These materials were lately implemented into a proton range phantom and results showed the materials are not tissue-equivalent for range calculations within clinical treatment planning systems (TPS) (Cook *et al* 2022).

The aim of this work is to develop end-to-end audit phantom materials to be used to mimic the patient workflow from patient data acquisition and treatment planning to dose verification. For the phantom material to be used through the workflow of a patient undergoing proton therapy, the materials need to be tissue-equivalent for both imaging photon energies as well as therapeutic proton energies to ensure the material is correctly characterised and provides accurate dosimetry of the target tissue. To our knowledge, this is the first model that enables the formulation of tissue-equivalent materials which considers not only photon interactions but also proton stopping power, nuclear absorption, and scattering interactions. The tissue-equivalence of the optimised materials were also compared against existing commercial tissue-equivalent materials to evaluate the performance of the latter and the improvement achieved with the new materials. Through the use of this model, new epoxy-resin based bone and muscle materials were made at the Barts Health NHS Trust using the manufacture process based on the work by White (1977). These manufactured materials were characterised by Monte Carlo simulations and experimental testing to assess their suitability for clinical use.

2. Methods

2.1. Epoxy-resin-based manufacture

In this study, the tissue-equivalent materials developed were based on epoxy-resin base mixtures (White *et al* 1977, Constantinou 1978, White 1974, 1977, 1978). The manufacture of epoxy resin-based tissue substitutes has been well described by White (1977). In summary, for the development of tissue-substitute materials, an epoxy resin, hardener, and selected powders or liquids are mixed to achieve a formulation with the required radiation properties of a desired target tissue. For successful hardening of the tissue-equivalent material, a specific mix ratio of epoxy resin and hardener is required; the different epoxy resin and hardener ratios are defined by White (1974) and were given the names CB1, CB2, CB3 and CB4. In this work, CB4 was used as that combination has

been thoroughly tested (White 1974) and can be used to produce larger cast volumes required for phantom development (White 1977). Typically, the mass density of epoxy resins are greater than that of soft tissue (Xu and Eckerman 2009), hence low density microspheres, such as phenolic microspheres, are typically added to the mixture to achieve the required mass density of the material without significant change to the elemental formulation (White 1977). The mixture is vacuumed during and/or after mixing to remove any possible air bubbles and left to cure over a few days.

2.2. Mathematical model

The aim of the model was to find which material ratios produce adequate target tissue mimicking properties for photon imaging beams as well as therapeutic proton beams. A list of 89 components was created based on the work of White (1974) and Constantinou (1978). The selected components were affordable (<£2 per gram) and non-hazardous. To create a material, CB4 was mixed with phenolic microspheres and N additional components. The mass ratios in which the epoxy, phenolic microspheres, and components are mixed dictate the final radiation properties of the mixture.

2.2.1. Mass density

The mass density of the material, ρ_m , needs to be mimicked to ensure that beam characteristics such as photon attenuation and proton range are the same as the target tissue. The conservation of volumes for material mixtures was assumed, which implies that no air is added into the mixture, that solid powders dissolve into the liquid without reducing the total volume and that chemical reactions also do not alter the volume. This results in the following formulation for the material's mass density:

$$\rho_m = \left(\sum_{i=1}^I \frac{w_i}{\rho_i}\right)^{-1}.\tag{1}$$

The index *i* represents one of the *I* mixture materials, and w_i , ρ_i are respectively the mass fractional weight and mass density of the material constituents of the mixture.

2.2.2. Mass attenuation coefficient

For photon interactions, the photon mass attenuation coefficient of the material, $\left(\frac{\mu}{\rho}\right)_m$, is the main beam interaction that needs to be considered for CT imaging (Andreo *et al* 2017). For mixtures, it is obtained as

$$\left(\frac{\mu}{\rho}\right)_{m} = \int \Psi(E) \sum_{i=1}^{I} w_i \left(\frac{\mu(E)}{\rho}\right) dE, \tag{2}$$

where $\left(\frac{\mu(E)}{\rho}\right)_i$ is the energy-dependent mass attenuation coefficient of the i^{th} material in the mixture, and $\psi(E)$ is the normalised spectrum of the polyenergetic x-ray source used for imaging. A 100 kVp clinical spectrum was used in the model.

2.2.3. Hounsfield unit

Multiplying $\left(\frac{\mu}{\rho}\right)_m$ with the density provides the linear attenuation coefficient of the material, μ_m , which can be used to calculate the HU of the material:

$$HU_m = 1000 \times \frac{\mu_m - \mu_w}{\mu_w},\tag{3}$$

where, μ_w is the linear attenuation coefficient of water. The HU is the quantity used to calculate the respective RSP of the material via the stoichiometric calibration curve (Schneider *et al* 1996).

2.2.4. Relative stopping power

The electronic stopping power $(S_e)_m$ is calculated via the Bethe equation assuming that other terms in the stopping power expression do not play a significant role in the clinical proton energy range

$$(S_e)_m = \frac{\rho_m 4\pi r_e^2 m_e c^2}{u} \frac{1}{\beta^2} \left(\frac{Z}{A} \right)_m \left[\ln \left(\frac{2mc^2 \beta^2}{(1 - \beta^2)I_m} \right) - \beta^2 \right], \tag{4}$$

where r_e is the electron radius, m_e is the electron rest mass, c the speed of light, u is the atomic mass unit, and β is the proton velocity in units of the velocity of light. $\left(\frac{Z}{A}\right)_m$ of the material was calculated using the rule of mixtures, where Z and A respectively represent the atomic number and atomic mass of the mixture. I_m is the mean excitation energy of the mixture in the condensed phase calculated using the Bragg additivity rule (ICRU 1993):

$$\ln\left(I_{m}\right) = \frac{\sum_{i=1}^{I} w_{i} \left(\frac{Z}{A}\right)_{i} \ln\left(I_{i}\right)}{\left(\frac{Z}{A}\right)_{m}}.$$
(5)

The mass electronic stopping power was determined over the energy range 50-250 MeV and then averaged. The average RSP of the mixed material, RSP_m, is calculated as the ratio of the electronic stopping power of the material to that of water:

$$RSP_{m} = \frac{(S_{e})_{m}}{(S_{e})_{w}}.$$
(6)

2.2.5. Nuclear interactions

Firstly, the nuclear reaction cross-section was calculated as it represents the probability of a primary proton being removed from the beam by a nuclear interaction. The linear energy transferred to secondary protons and alpha particles was also calculated at low and high proton beam energies ($E_1 = 50$ and $E_2 = 200$ MeV). Secondary proton and alpha particles were chosen because those are the secondary particles that contribute most significantly to dose in low-Z materials (Lourenço *et al* 2016). Cross-section data from ICRU Report 63 were used (ICRU 2000).

The nuclear reaction cross section of the mixture at energy E_p per atomic mass, $\left(\frac{\sigma_{\text{nucl}}(E_p)}{A}\right)_m$, in units of cm² g⁻¹, was calculated with the rule of mixtures (ICRU 2000):

$$\left(\frac{\sigma_{\text{nucl}}(E_p)}{A}\right)_m = \sum_{i=1}^{I} w_i \left(\frac{\sigma_{\text{nucl}}(E_p)}{A}\right)_i. \tag{7}$$

The linear energy transferred from a proton of energy E_p to a secondary particle k, where k is a proton or an alpha particle, is defined as $\left(\frac{\sigma_{\text{tr,}k}(E_p)}{A}\right)_{\text{tr.}}$ with units of MeV cm² g⁻¹, is calculated using:

$$\left(\frac{\sigma_{\text{tr},k}(E_p)}{A}\right)_m = \sum_{i=1}^I w_i \left(\frac{\sigma_{\text{tr},k}(E_p)}{A}\right)_i \bar{W}_k(E_p) ,$$
(8)

where $\bar{W}_k(E_p)$ is the average emission energy of the recoil spectrum.

The sum of the nuclear interactions cross sections value was calculated to give them equal weighting in the cost function:

$$\left(\frac{\bar{\sigma}_{\text{nucl}}}{A}\right)_{m} = \sum_{E_{p}=50,200 \text{ MeV}} \left[\left(\frac{\sigma_{\text{nucl}}(E_{p})}{A}\right)_{m} + \left(\frac{\sigma_{\text{tr,proton}}(E_{p})}{A}\right)_{m} + \left(\frac{\sigma_{\text{tr,alpha}}(E_{p})}{A}\right)_{m}\right].$$
(9)

2.2.6. Scattering length

The elemental scattering length, $X_{s,i}$ was estimated as (Gottschalk 2010):

$$\frac{1}{\rho X_{s,i}} = \alpha N_A r_e^2 \left(\frac{Z^2}{A}\right) \left(2\log(33219(AZ)^{-\frac{1}{3}}) - 1\right)$$
 (10)

where α is the fine structure constant and N_A is Avogadro's constant. The scattering length of mixtures is obtained with equation (11):

$$\left(\frac{1}{\rho X_s}\right)_m = \sum_{i=1}^I w_i \left(\frac{1}{\rho X_s}\right)_i \tag{11}$$

2.2.7. Cost function

A cost function was established to quantify the similarity between a mixture and a target material. The cost function is a weighted sum of the square of relative differences between 6 properties of the target and mixture material. The 6 quantities (noted with index q) are the mass density ρ_m (equation (1)), mass attenuation coefficient $\left(\frac{\mu}{\rho}\right)_m$ (equation (2)), HU_m (equation (3)), relative stopping power RSP_m (equation (6)), scattering length $X_{s,m}$ (equation (10)) and sum of nuclear interaction cross sections (equation (9)). Ultimately, all properties depend upon the mass fractional weights w_i of the I components of the mixture, which are the optimisation variables. The cost function is defined as

$$C(w_i) = \sum_{q=1}^{6} \delta_q \Delta_q^2, \tag{12}$$

where Δ_q is the relative difference on the q^{th} quantity between target material and the proposed mixture, and δ_q is an empirically defined weighting of the relative importance of each quantity (see table 1). Mass density, mass attenuation and RSP were assigned higher weights due to their impact on the materials ability to be correctly characterised during imaging and TPS planning as well as providing accurate proton dosimetry and range measurements.

The optimisation of the new formulation was achieved by finding a local minimum of the cost function using a constrained nonlinear least squares algorithm. The model was implemented in Matlab R2020b (MathWorks, Natick, MA, U.S.A.). The function was constrained by two conditions mainly linked to the manufacturing process for epoxy resin-based materials:

- (i) A minimum of $w_i = 60\%$ CB4 was set as the lower limit for the epoxy resin in the model. This ensures that the components would be mixable and pourable in the manufacturing stage.
- (ii) Overall, the formulation was set either I=3 or 4 parameters to optimise (mass fractional weight of CB4, mass fractional weight of phenolic microspheres and mass fractional weight of one or two mixture component). The number of mixture components was set to either N=1 or 2 component per mixture to reduce the complexity of the manufacture process. Phenolic microspheres were always considered in the mixture formulation to easily ensure matching the density of the targeted material.

The optimal material was selected as the one with the lowest cost function.

2.3. Implementation of the mathematical model

The main challenge was to formulate materials that could be successfully mixed and poured, and that resulted in a homogeneous final material. Although the model provides a fast method for the formulation of theoretical proton optimised tissue-equivalent materials, the manufacture process remained a trial-and-error method and multiple materials were developed during this study. This was mainly due to the selected component powders not being fine enough to ensure homogeneous mixing into the CB4 mixture; crystalline powders were shown to sink during the curing process. Consequently, the number of components used from the library was constantly revised during the study as selected powders were shown to be unsuccessful in the mixing process.

The model was used to formulate a vertebra bone-equivalent (two samples were formulated, VB#1–2) and skeletal muscle-equivalent material (five samples formulated, MS#1, MS#2, MS#3, MS#3 v2 and MS#H) based on Woodard and White (Woodard and White 1986) and ICRP reference tissue data (Snyder *et al* 1975). Photon and proton interactions were also calculated for current commercial tissue-equivalent materials (CIRS Inc. (CIRS 2020), Leeds Test Object (Leeds Test Objects 2014), and Gammex Inc. (Sun Nuclear 2019) against selected human tissues. For commercial materials, the material density and elemental composition data was taken from published documentation (Leeds Test Objects 2014, Goma *et al* 2018). Table 1 shows the material formulation input settings and cost function weightings (δ_q) for each quantity (q) considered in the model for each mixture.

For VB#1–2 and MS#1, the cost function weighting for HU was set to zero due the initial model only considering the spectrum weighted mass attenuation parameter. These first formulations highlighted the importance of accurately matching the HU quantity to ensure correct TPS RSP assignment. Consequently, for MS#2–3, a weighting value was used for HU in the cost function. Also, after the manufacture of MS#3, the formulation was adjusted by the addition of less than 1% of phenolic microspheres to alter the density to better mimic the target tissue density, this formulation was named MS#3 v2. During the study, the development of a homogenous muscle was shown to be challenging, due its importance in the photon imaging and TPS characterisation stage, a less optimised but more homogenous mixture was developed called MS#H.

2.4. Monte Carlo validation of the mixtures

Monte Carlo simulations were performed for validation of the theoretical radiation properties of the materials calculated via the mathematical model by simulating a proton beam travelling through a given thickness of human tissue and tissue-equivalent materials. Monte Carlo simulations were performed with FLUKA 2021.2.1 and Flair 2.3.0 (Vlachoudis 2009, Battistoni *et al* 2015, Ahdida *et al* 2022). The range, RSP, and fluence correction factor were evaluated with the Monte Carlo simulations, as defined in sections 2.4.1 and 2.4.2. For each simulation, 6×10^6 proton histories were tracked and the beam was modelled as a mono-directional 200 MeV pencil beam. The default settings for particle therapy were used with full transport of ions (inelastic scattering, elastic scattering, and nuclear interactions) while secondary electrons were set to deposit dose locally. The transport cut-off energies for proton and heavier particles were set to 100 keV. The elemental composition,

Table 1. Description of material formulation input settings and cost function weighting, δ₀, used for each formulation. For VB#1 and MS#H, the compound library was limited to only components used in current manufacture of photon tissue-equivalent materials at Barts Health NHS Trust (White 1974) or had been shown to mix well during the study. For the other iterations, VB#2, MS#1-3 the full component library was considered minus the powder previously used in earlier formulations.

			Cost function weighti							
Name of material formulation	Target tissue	Component library (<i>N</i>)	Component properties	N	Spectrum weighted mass Density attenuation		RSP Scattering length		Average nuclear interaction	HU
VB#1	Vertebra Column (C4) (excluding cartilage)	3	Fine powders	1	0.21	0.26	0.26	0.13	0.13	0
VB#2		89	Liquid and powders	1	0.21	0.26	0.26	0.13	0.13	0
MS#1	ICRP Skeletal Muscle 2	89	Liquid and powders	1	0.21	0.26	0.26	0.13	0.13	0
MS#2		88	Liquid and powder	1	0.17	0.22	0.22	0.11	0.11	0.17
MS#3		87	Liquid and powders	1	0.17	0.22	0.22	0.11	0.11	0.17
MS#H		4	Fine powders	2	0.5	0.5	0	0	0	0

density, and theoretical calculated *I*-value of the materials were entered into the material information. For newly formulated materials, the mathematical model derived theoretical density was used. Existing commercial bone and muscle solutions were also assessed. All materials were modelled as homogeneous within the simulations. A cylindrical target of radius 30.0 cm and thickness of 26.0 cm was modelled, and the total dose was scored in 0.2 cm thick slabs throughout the target. The dose distribution and fluence for primary protons, secondary protons, alpha, He³, deuterons and tritons were scored throughout the cylinder.

2.4.1. Range and RSP

The percentage depth dose (PDD) for the proton beam in each material was calculated. The range was determined from the PDD and was defined as the R_{80} , the depth distal to the Bragg peak where the PDD drops to 80%. The range also provides the RSP (RSP $_m^{MC}$), which is determined by the following equation:

$$RSP_m^{MC} = \frac{R_{80,w}^{MC}}{R_{80,m}^{MC}},$$
(13)

where $R_{80,w}^{\text{MC}}$ is the distal R_{80} range in water and $R_{80,m}^{\text{MC}}$ is the distal R_{80} range in the target material.

2.4.2. Fluence correction factor

The fluence correction factor, $k_{\rm fl}^{\rm MC}$, provides information on the difference in fluence between materials (Palmans $et\,al\,2013$, Lourenço $et\,al\,2016$), and was calculated as described in Palmans $et\,al\,(2013)$. The fluence difference provides an understanding of the differences in non-elastic nuclear cross sections of the material compared to the target tissue. Consequently, if $k_{\rm fl}^{\rm MC}=1$, this suggests that the material and target tissue are equivalent in terms of particle fluence (Palmans $et\,al\,2013$).

2.5. Experimental validation of the mixtures

The formulations were manufactured by the Barts Health NHS Trust and a series of tests were performed at the National Physical Laboratory (NPL, UK), University College London Hospital Proton Centre (UCLHPC), and the Rutherford Cancer Centre Thames Valley (RCCTV) to characterise the materials to ensure they were within suitable uncertainties for use in proton therapy. For each formulation, three blocks were manufactured with the following dimensions: $10 \text{ cm} \times 10 \text{ cm}$ slabs of 0.5 cm, 1.0 cm and 2.0 cm thickness.

2.5.1. Density

The measured material density of the three individual slabs was calculated by weighing them on a Mettler Toledo analytical balance (Model PG503 S) and performing length measurements with Mitutoyo Absolute IP 67 digital callipers (Model CD 8PSX).

2.5.2. Relative Stopping Power

Measurements were taken at UCLHPC using a mono-energetic proton beam. The IBA Giraffe device (IBA Dosimetry) was used to provide a complete PDD curve in one irradiation. For VB#1-2 a 140 MeV proton beam was used. For MS#1-3 and MS#H, a 200 MeV proton beam was used. It should be noted that water-equivalent thickness measurements do not depend significantly on energy over the clinical proton energy range (Zhang and Newhauser 2009).

At both energies, a reference PDD was initially taken without an additional material (figure 1, setup 1). Then each slab of material was placed in front of the entrance window of the detector, and the PDD measurement repeated for each material (figure 1, setup 2). PDD measurements were performed to determine the water equivalent thickness (WET_m), and RSP of the materials (RSP^{Exp}_m), using equations (14) and (15), respectively (Newhauser and Zhang 2015).

$$WET_{m} = R_{80,w}^{Exp} - R_{80,w,m}^{Exp}$$
 (14)

$$RSP_m^{Exp} \approx \frac{WET_m}{t_m} \tag{15}$$

 $R_{80,w}^{\rm Exp}$ corresponds to the range in water, $R_{80,w,m}^{\rm Exp}$ is the R_{80} range in water when including the material slab in front of the water phantom and $t_{\rm m}$ the thickness of the material slab. The R_{80} values were determined via the IBA detector software which applied the Bortfeld fit to the Bragg peak curve before interpolating the R_{80} range (Bortfeld 1997). Thickness measurements of the slabs was determined by dimensional measurements (section 2.5.1).

2.5.3. Single-energy CT and Dual-energy CT

Each slab was scanned in a Mediso AnyScan SCP scanner at the NPL. The samples were placed centrally within custom made inset within bolus sheets and solid water was placed above and below the setup on the carbon fibre

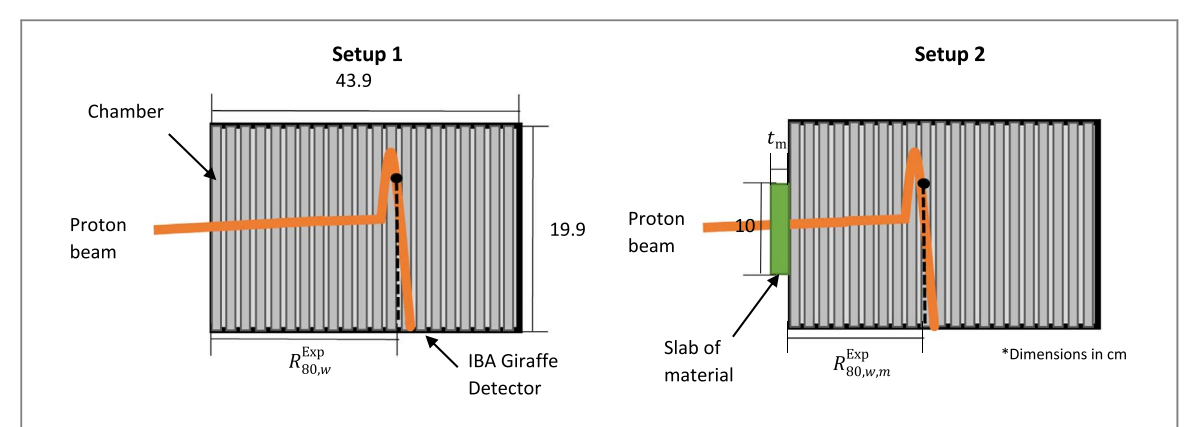
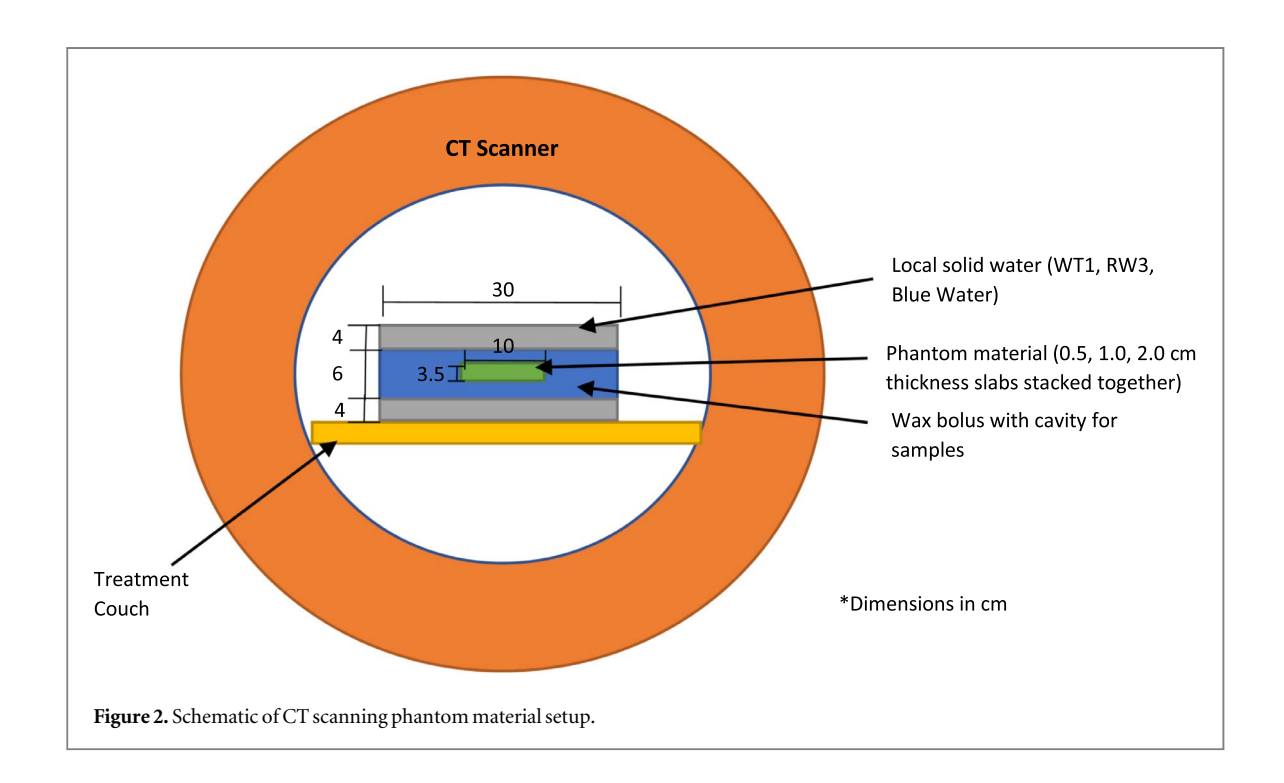


Figure 1. Experimental setup for water-equivalent thickness measurements (without - setup 1, left - and with - setup 2, right – phantom material in front of the Giraffe detector). The number of ionization chambers shown within detector is reduced to simplify the schematic.



CT couch (figure 2). This custom made inset for the samples was developed to reduce scattering and artefacts in the scan due to air. The following scanner settings were used; axial scan, 80 kV, 100 kV, 120 kV and 140 kV tube voltages, voxel size of $0.098 \times 0.098 \times 0.125$ cm³, tube current of 300 mA and scan reconstruction of abdomen. Each slab (0.5 cm, 1.0 cm, and 2.0 cm) was scanned separately as well as scanned together as a $10 \text{ cm} \times 10 \text{ cm} \times 3.5 \text{ cm}$ block.

CT scans were also performed on two clinical CT scanners; the Philips CT 7500 scanner at the UCLHPC and the Philips Big Bore CT scanner at the RCCTV, using 120 kV tube voltage and similar setting as the scans aforementioned.

2.5.3.1. Homogeneity

Homogeneity of the samples was tested through visual assessment of the single-energy CT (SECT) images taken at NPL. Visual examination looked for any air bubbles and marbling effects in slices from the CT images as well as assessment of the materials variability through HU standard deviation (SD) calculations for each sample. The SD of the HU values of the samples was compared to WT1 to quantitively assess their homogeneity. WT1 is a commercial photon solid water equivalent material that has been shown to be acceptably homogeneous and it is extensively used in conventional radiotherapy. A plastic bottle filled with distilled water was also scanned alongside the samples to provide information on HU variation due to CT scanner noise.

2.5.3.2. HU and CT-based RSP estimation

Raystation 10B (version 10.1.100) was used to determine the HU of the material by manual contouring the central regions of each slab. The average HU values of the materials were derived from taking the HU value of the individual slabs (0.5 cm, 1.0 cm and 2.0 cm) as well as the combined 3.5 cm thick slab setup. The HU values for the three individual slab thicknesses were then applied to the stoichiometric calibration curves and the average predicted RSP $_m^{\rm TPS}$ and respective SD were determined for each scanner. At NPL, SECT and Dual-energy CT (DECT) analysis was completed to predict RSP $_m^{\rm TPS}$. For DECT, the stoichiometric method of (Bourque *et al* 2014) was applied to the 100 kV and 140 kV scan data. The assigned RSP $_m^{\rm TPS}$ were then compared to experimentally derived RSP $_m^{\rm Exp}$ values.

3. Results

3.1. Mathematical model calculations

Table 2(a) shows the relative difference of physical and radiation parameters between the new vertebra bone formulations and commercial bone materials against human vertebra bone. Similarly, table 2(b) shows the relative difference of physical and radiation parameters between the new skeletal muscle formulations and commercial muscle materials against the skeletal muscle. A cost function value of zero would suggest that all radiation parameters match to the target tissue.

3.2. Validation of material radiation parameters

3.2.1. Monte Carlo simulations

3.2.1.1. Range and RSP measurements

The relative difference between the mathematical model and Monte Carlo simulation predicted RSP was 0.4% (SD = 0.4%). Figure 3 shows $R_{80,m}^{\rm MC}$ and RSP $_m^{\rm MC}$ values determined from the simulation for the VB#1–2, MS#1–3 and MS#H, and commercial tissue-equivalent materials as well as their corresponding target tissues, vertebra bone, and skeletal muscle for a 200 MeV proton beam.

3.2.1.2. Fluence correction factors

Figure 4 shows the fluence correction factor of each newly formulated material and commercial materials for each target material. The depth was scaled to the range of the target tissue.

Table 2. (a) Comparison of new formulations and commercial bone materials against vertebra bone, (b) comparison of new formulation and commercial muscle materials against skeletal muscle. For the cost function (1), the weightings shown in table 1 for formulations VB#1–2 and MS#1 were used and for cost function (2) the weighting shown in table 1 for MS#2–3 were used which included a HU weighting.

Relative % difference to target tissue		VB#1	VB#2	CIRS Bone 800 mg/ c.c. HA	Gammex Bone #480	Gammex Bone #484	Leeds test object (Average bone)
a							
Mass density		1.41	0.70	7.75	9.86	-5.99	-1.41
Mass attenuation coefficient		1.16	0.46	18.83	8.09	-10.90	-6.96
RSP		-0.12	-0.67	6.63	8.20	-4.02	-0.85
Scattering length		1.02	0.54	-11.45	-10.20	20.57	10.85
Average nuclear interactions		2.61	1.65	1.82	1.57	5.42	4.47
Cost function (1)		1.79	0.66	133.66	68.76	101.43	31.09
Relative % difference to target tissue	MS#1	MS#	2	MS#3	MS#H	CIRS Muscle	Gammex Muscle
b							
Mass density	1.90	0.95		0.95	0.00	1.14	0.00
HU	65.61	0.25		-0.54	0.00	1.53	-18.71
Mass attenuation coefficient	1.00	-0.93	3	-0.97	0.00	-1.06	-0.83
RSP	-1.34	-1.20)	-1.16	-0.35	1.28	-1.18
Scattering length	0.62	7.60		7.67	10.87	11.24	10.51
Average nuclear interactions	2.86	4.93		5.06	5.48	5.84	5.44
Cost function (1)	2.61	11.46		11.76	19.29	21.86	18.75
Cost function (2)	N/A	9.70		9.99	16.32	18.88	75.39

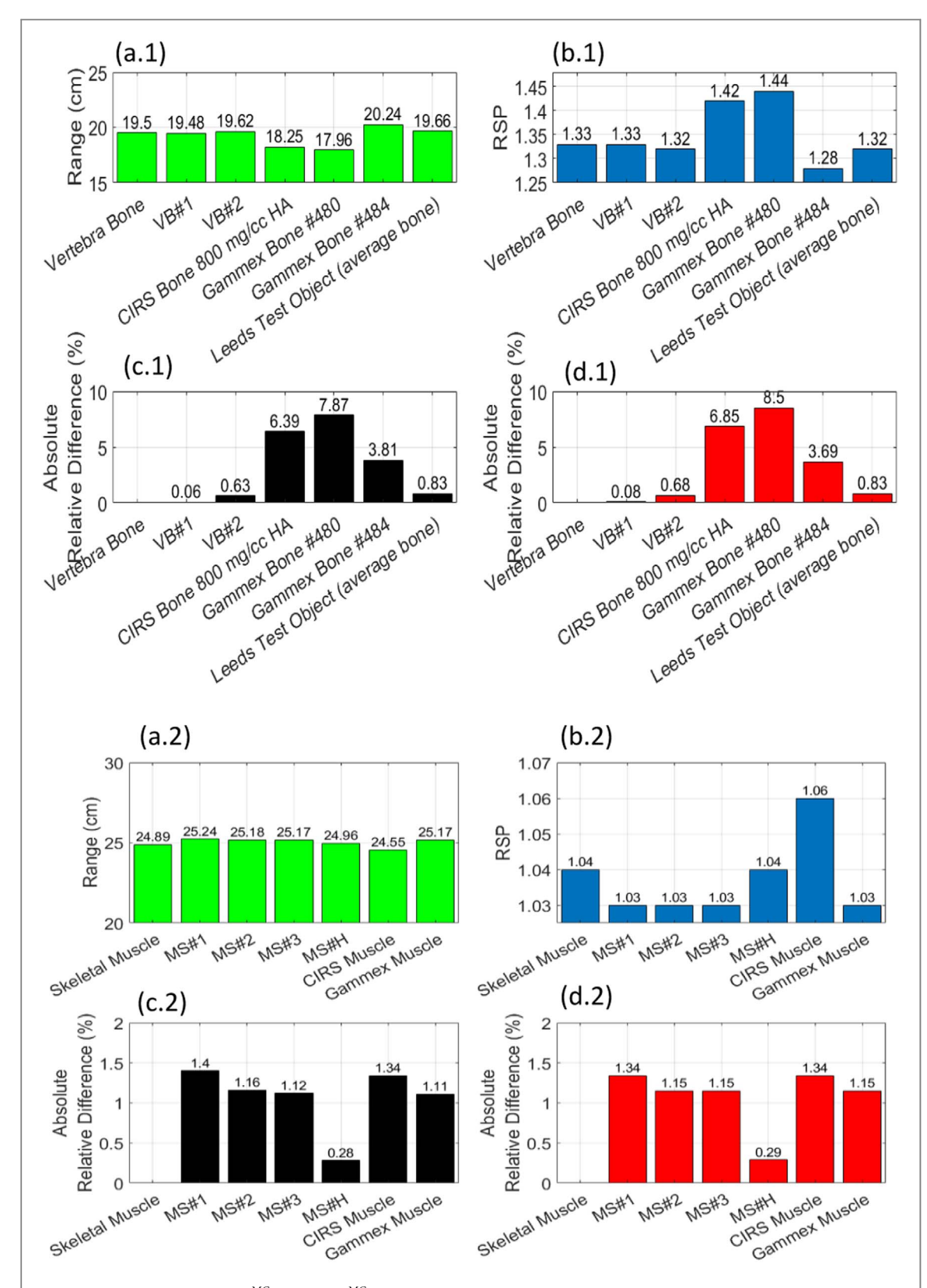


Figure 3. Monte Carlo derived $R_{80,m}^{\rm MC}$ and RSP $_m^{\rm MC}$ values of all new formulations (VB#1-2, MS#1-3 and MS#H) and commerical materials for a 200 MeV proton beam. $R_{80,m}^{\rm MC}$ values for vertebra bone and vertebra bone plastics are presented in figure 3(a.1) while $R_{80,m}^{\rm MC}$ values for muscle, and muscle plastics are presented in figure 3(a.2). Their respective relative difference to the target tissue are presented in figures 3(c.1) and (c.2). RSP $_m^{\rm MC}$ values for vertebra bone plastics are presented in figure 3(b.1) while RSP $_m^{\rm MC}$ values for muscle plastics are presented in figure 3(a.2). Their respective relative difference to the target tissue is presented in figures 3(d.1) and 3(d.2).

3.2.2. Measurements

3.2.2.1. Homogeneity

Table 3 and figure 5 shows the HU values and CT scans of each new formulation. Although no material showed air bubbles, heterogeneity of samples can be seen in the scans. For MS#1, the setting of the component powder

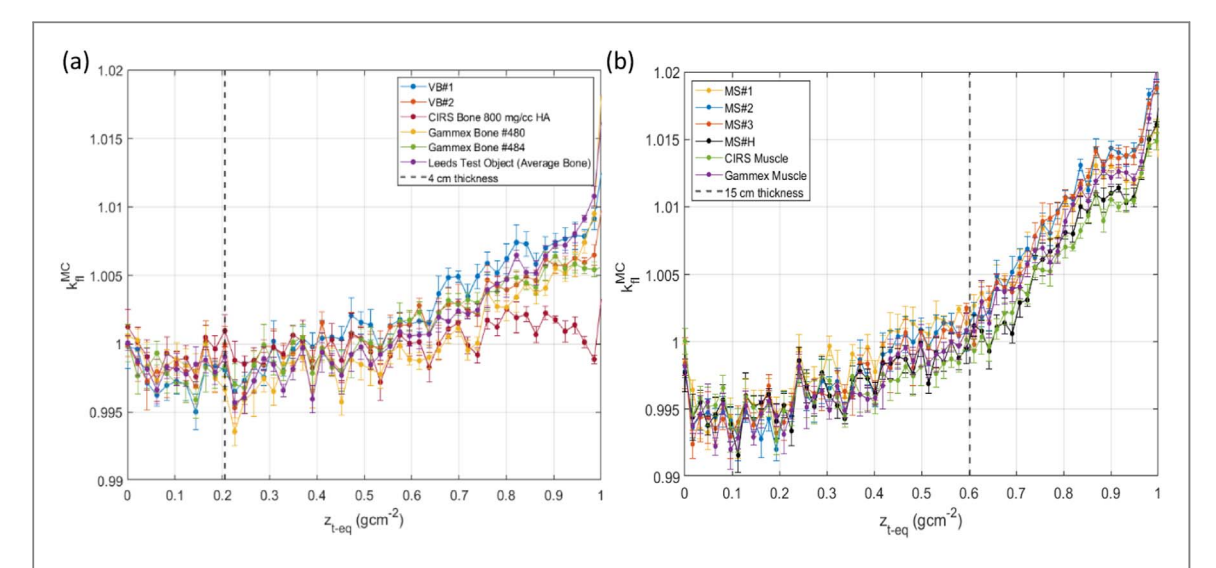


Figure 4. Fluence correction factors for new formulations and commercial materials. (a) Vertebra bone tissue-equivalent materials (b) muscle tissue-equivalent materials. Reference dashed lines highlighted maximum tissue thicknesses of each target tissue a proton may pass through in a patient (4 cm for bone and 15 cm for muscle). Type A uncertainties are presented with each error bar.

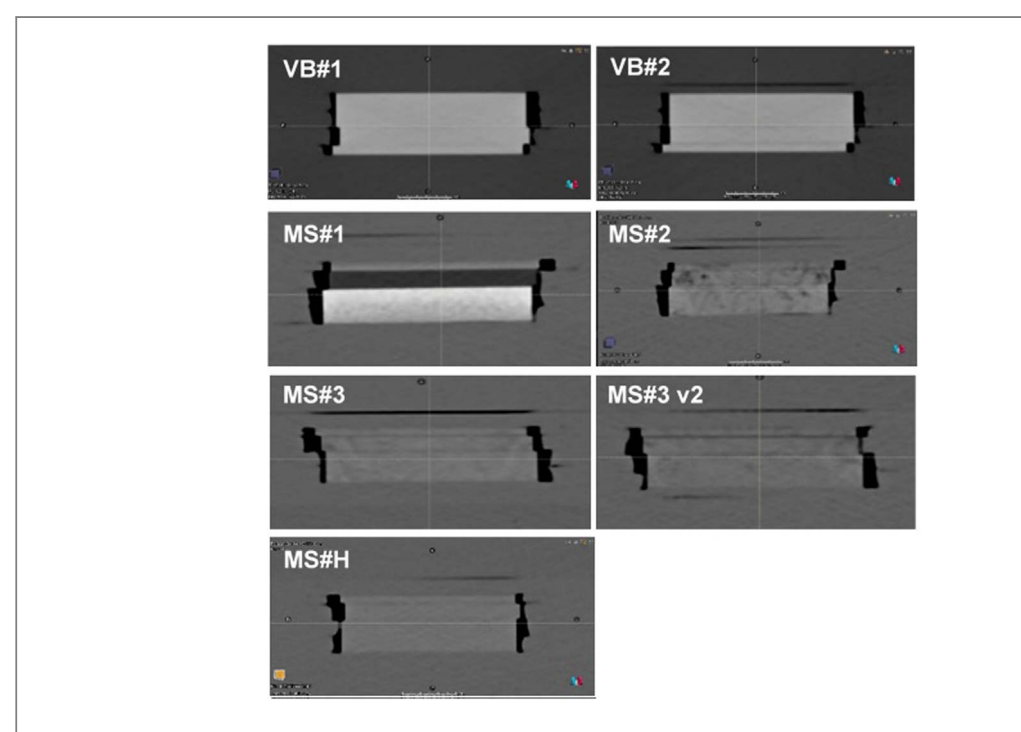


Figure 5. Example CT slices of new formulations.

Table 3.~HU~values~(max,min,average~and~SD).

		_		
Material	Min HU	Mean HU	Max HU	SD
WT1	-38	9.17	44	8
VB#1	546	634	705	20
VB#2	490	611	675	20
MS#1	-178	82	439	190
MS#2	-388	47	141	59
MS#3	-44	52	110	21
MS#3 v2	-116	26	86	24
MS#H	6	48	79	10

within the sample is clearly visible in figure 5. A SD level of 5 HU was attributed to scanner noise through investigating HU variation for a reference water bottle placed alongside the material scans.

3.2.2.2. Density and RSP $_m^{Exp}$ measurements

Table 4 shows the experimental calculated mass density and RSP $_m^{\rm Exp}$ values for the new formulations, as well as relative difference to model-predicted values and to target tissues values. The mathematical model on average predicted the experimental material density within 1.3% (SD = 0.8%) and RSP within 2.5% (SD = 0.9%) when MS#1 is excluded. MS#1 shows significant variation in density between measured slabs due to its heterogeneous nature (figure 4(c)). For the vertebra bone materials, the experimental values were on average within 2.0% (SD = 0.6%) for mass density and RSP with target human vertebra bone formulation. For the muscle materials, the experimental values were on average within 1.7% (SD = 1.1%) for mass density and RSP with target human skeletal muscle formulation. For MS#3 and MS#3 v2, the addition of phenolic microspheres reduced the percentage point difference to the target skeletal muscle by 1.7 for mass density and 2.4 for RSP.

3.2.2.3. HU and CT-based RSP estimation

Table 5 compares predicted RSP $_m^{\text{TPS}}$ (using the CT stoichiometric calibration) from NPL, UCLHPC, and RCCTV, against experimental RSP $_m^{\text{Exp}}$ values taken at UCLHPC (section 2.5.2.). The table shows that at NPL, for all materials the RSP $_m^{\text{TPS}}$ can be assigned on average within 1.4% (SD = 0.5%) difference to the experimental RSP $_m^{\text{Exp}}$ when using single-energy CT. This is reduced to, on average, within 1.3% (SD = 0.5%) if dual energy CT is used. At UCLHPC, for all materials the correct RSP $_m^{\text{TPS}}$ can be assigned on average within 2.3% (SD = 0.9%) difference to experimental RSP $_m^{\text{Exp}}$ and for the RCCTV all materials can be assigned the correct RSP $_m^{\text{TPS}}$ within 1.9% (SD = 1.3%) difference to experimental RSP $_m^{\text{Exp}}$.

4. Discussion

Table 2 and figure 3 highlight the overall potential of the new formulations to perform better than current commercial tissue-equivalent materials. Table 2 shows new formulations score well (close to zero) via the weighted cost function which indicates their feasibility for providing improved proton dosimetry. Results also suggest good agreement between the mathematical model and Monte Carlo simulations values, where for RSP_m^{MC} were on average within 0.35%. Figure 3 indicates that all formulated materials match the target tissue ranges within 0.78% whereas commercial bone materials showed to have a relative difference up to 8% for range.

However, unlike the mathematical model predictions of improved nuclear interactions, Monte Carlo shows the fluence correction of the new formulations are comparable to commercial tissue-equivalent materials. Therefore, this suggests a higher weighting of the nuclear interaction parameters may be necessary or the current parameter does not fully capture the nuclear interactions of the targeted material. Some uncertainty can be attributed to the nuclear data used in the model compared to Monte Carlo simulations. The model uses ICRU Report 63 data which reports uncertainties of the order 5%–30% for cross sectional data; whilst for FLUKA, the PEANUT nuclear model was used which uses a blend of experiment data, data driven theoretical approaches, particle data group fits and phase shift analysis (Ferrari and Sala 1993). Work by Lourenço *et al* 2017 reported at least 2% differences in fluence correction factors depending on the Monte Carlo code. Previous research has also highlighted the challenge of quantifying the probability of non-elastic nuclear interactions due to hydrogen content of compounds (Rasouli *et al* 2016). Consequently, consideration should be made to adapt the model to improve the optimisation of nuclear interactions.

From table 2, VB#1-2, MS#1 were shown to provide the best optimisation of radiation parameters, however, manufacture challenges meant formulations did not result in suitable homogenous mixtures. Figure 5 highlights the unsuccessful mixing of MS#1 into a homogenous mixture due to the powdered material settling within the mixture whilst it hardens. MS#1-2 showed (table 3) significant variation in HU from the mean which suggests that these materials should not be used for clinical phantom use. Significant HU variation of the material is an undesirable material trait for certain applications such as phantoms for reference dosimetry and profile measurements. However, for the use in anthropomorphic phantom for end-to-end audits, minor HU variation could be useful as this would simulate human tissue heterogeneity. This could provide rigorous testing of the TPS and dose calculations during the patient workflow audit. Nevertheless, the challenge of inhomogeneous plastics is capturing HU variation which is clinically relevant and distinguished within the CT image.

After a review of muscle iterations and the available powders, the optimisation was simplified and focused on the manufacture of a homogeneous material, MS#H. The development of a homogeneous material was at the

H Cook et al

Table 4. Mass density and RSP measurements of samples.

Material	VB#1	VB#2	MS#1	MS#2	MS#3	MS#3 v2	MS#H
Average mass density (SD)	1.458 (<0.01)	1.443 (<0.01)	1.091 (0.19)	1.056 (0.04)	1.080 (0.01)	1.055 (0.02)	1.054 (<0.01)
Average relative % difference to model prediction (SD)	1.25 (0.24)	0.91 (0.25)	12.21 (8.97)	2.67 (1.43)	1.79 (0.98)	1.04(0.22)	0.36(0.11)
Average relative % difference to target tissue (SD)	2.69 (0.25)	1.62 (0.25)	13.21 (8.95)	2.37 (2.20)	2.85 (1.03)	1.11 (1.13)	0.37 (0.11)
Average RSP_m^{Exp} (SD)	1.354 (< 0.01)	1.342 (<0.01)	1.058 (0.16)	1.052 (0.01)	1.067 (0.01)	1.051 (0.01)	1.061 (<0.01)
Average relative % difference to model prediction (SD)	2.43 (0.23)	2.08 (0.06)	10.91 (6.47)	2.14(1.28)	4.34 (0.65)	2.08 (0.45)	2.21 (0.23)
Average relative % difference to target tissue (SD)	2.37 (0.24)	1.44(0.06)	10.66 (7.34)	0.98 (1.33)	3.33 (0.07)	0.91 (0.48)	1.90 (0.24)

H Cook et a

Table 5. Stoichiometric calibration results for SECT, DECT, and clinical CT. Due to MS#1 not being suitable for clinical use due to powder settling within sample, the sample was not CT scanned at UCLHPC and RCCTV.

Location and type of CT scan	Material	VB#1	VB#2	MS#2	MS#3	MS#3 v2	MS#H
NPL (SECT 120 kVp)	Average HU (SD)	633 (10)	609 (9)	50 (22)	52 (5)	26 (12)	48(1)
	Average RSP_m^{TPS} (SD)	1.377 (0.01)	1.364 (0.01)	1.049 (0.02)	1.054 (0.01)	1.034 (0.01)	1.051 (<0.01)
	Average relative % difference to experimental RSP_m^{Exp} (SD)	1.67 (0.61)	1.62 (0.43)	0.57 (0.61)	2.04 (0.67)	1.61 (0.66)	0.96 (0.23)
NPL (DECT (100 kVp and 140 kVp)	Average HU (SD)	704 (7) and	674 (4) and	52 (22) and	49 (5.4) and	24 (12) and	50 (1) and 46 (1)
		581 (12)	558 (11)	49 (22)	53 (6)	29(11)	
	Average RSP_m^{TPS} (SD)	1.355 (0.10)	1.346 (0.04)	1.049 (0.03)	1.060 (0.01)	1.035 (0.01)	1.050 (< 0.01)
	Average relative % difference to experimental RSP_m^{Exp} (SD)	0.64 (0.48)	1.91 (1.61)	0.94 (0.82)	1.50 (0.71)	1.57 (0.89)	1.10 (0.23)
UCLH Proton Centre DECT (120 kVp, dual- layer)	Average HU (SD)	692 (6)	662 (7)	47 (23)	41 (9)	16 (10)	46(1)
·	Average $RSP_m^{TPS}(SD)$	1.331 (<0.01)	1.318 (<0.01)	1.036 (0.02)	1.034(0.01)	1.020(0.01)	1.038 (<0.01)
	Average relative % difference to experimental RSP_m^{Exp} (SD)	1.70 (0.36)	1.74 (0.29)	1.46 (0.65)	3.89 (0.59)	3.00 (0.39)	2.24(0.23)
Rutherford Cancer Centre, Thames Valley (SECT 120 kVp)	Average HU (SD)	621 (11)	596 (10)	40 (22)	37 (6)	15 (9)	N/A
	Average $RSP_m^{TPS}(SD)$	1.345 (0.01)	1.330 (0.01)	1.037 (0.02)	1.036 (0.01)	1.022 (0.01)	N/A
	Average relative % difference to experimental RSP_m^{Exp} (SD)	0.69 (0.55)	0.88 (0.43)	1.38 (0.60)	3.77 (0.69)	2.76 (0.32)	N/A

cost of optimising the phantom material for proton interactions and resulted in a formulation with a smaller uncertainty on the assignment of RSP_m^{TPS} .

Overall, results from table 4 (excluding MS#1) indicated that the model can predict mass density and radiation properties within the relative standard uncertainty of the method of calculation. The model predicted the RSP and mass density of the materials within 1.5% (when RSP calculations are corrected for experimental density values). Table 4 also shows for both the vertebra bone and muscle materials, that formulations were on average within 2% for mass density and RSP $_m^{\rm Exp}$ of the human target tissues. Results indicate VB#2 and MS#3 v2 are the most suitable bone and muscle-equivalent materials and outperform many of the existing materials. Major improvements were achieved in comparison to commercial bone materials, which showed relative differences up to 10% and 8% respectively for mass density and RSP $_m^{\rm MC}$ (table 2).

The materials were also assessed for their use as phantom materials for audit purposes. As previously mentioned, the acceptance criteria of phantom materials for IROC phantom development (Grant $et\ al\ 2014$) is a 5% uncertainty in TPS assigned RSP. Results from SECT and DECT scans at NPL and clinical centres (UCLHPC and RCCTV) suggest the materials RSP $_m^{\text{TPS}}$ can be correctly assigned within 1%–3% (table 5). The improved homogeneity of MS#H also showed to improve the consistency and accuracy of RSP $_m^{\text{TPS}}$ assignment. Consequently, the optimised materials RSP $_m^{\text{TPS}}$ assignment is clearly within the 5% uncertainty IROC phantom material acceptance criteria and with certain phantom iterations the RSP $_m^{\text{TPS}}$ uncertainty is likely to be masked within the uncertainty of other steps in the phantom audit process such as setup and dosimeter measurement.

Future work will look to apply this model to manufacture proton optimised water and other human tissues (lung and denser bone) materials as well as be applied to support research into 3D printable based optimised materials.

5. Conclusion

The model developed is a powerful tool for the formulation of tissue-equivalent materials optimised for proton dosimetry. In previous research, Lewis *et al* (2018), existing bone materials have been shown to produce large uncertainties for range measurements. This work agrees with this finding as selected existing bone plastics have shown to produce up to 20% relative difference to the vertebra bone for key proton radiation parameters. This model enabled the creation of new proton optimised tissue-equivalent materials which are superior than current commercial bone and muscle materials when both mass density, photon interactions and proton interactions are determined via a weighted cost function.

Manufactured materials were characterised by Monte Carlo simulations and experimental testing and results suggest VB#2 and MS#3 v2 are the most tissue-equivalent (within 2% relative difference for key radiation parameters) and perform better than existing tissue-equivalent materials. The materials were also tested as audit materials by comparing stoichiometric calibration predicted and experimental determined RSP. Overall, for the new materials formulated, TPS predicted the experimental RSP values within 1%–3%, and consequently they can be used as clinical phantom materials. VB#2, MS#3 v2, and MS#H as well as future materials developed by the model will be used within clinical phantoms to improve phantom dosimetry measurements.

Acknowledgments

The authors would like to thank the medical physicists and proton beam engineers at University College London Hospital, Proton Centre and The Rutherford Cancer centre, Thames Valley for their assistance during the experiments. As well as the Barts Health NHS Trust staff for helping in the manufacture of the new phantom materials. This work was supported by the National Measurement System of the UK's Department for Business, Energy, and Industrial Strategy.

ORCID iDs

H Cook https://orcid.org/0000-0002-3306-9704

M Simard https://orcid.org/0000-0003-0610-6319

G Royle https://orcid.org/0000-0002-8548-7684

H Palmans https://orcid.org/0000-0002-0235-5118

A Lourenço https://orcid.org/0000-0001-6829-3338

References

Ahdida C et al 2022 New capabilities of the FLUKA multi-purpose code Front. Phys. 9 788253
Al-Sulaiti L, Shipley D, Thomas R, Owen P, Kacperek A, Regan P H and Palmans H 2012 Water equivalence of some plastic-water phantom materials for clinical proton beam dosimetry Appl. Radiat. Isot. 70 1052–7

```
Andreo P, Burns DT, Hohlfeld K, Huq MS, Kanai T, Laitano F, Symth V and Vynckier S 2000 IAEA TRS-398 Absorbed Dose Determination in External Beam Radiotherapy: An International Code of Practice for Dosimetry based on Standards of Absorbed Dose to Water. (Austria: IAEA) Andreo P, Burns DT, Nahum A E, Seuntjens J and Attix F H 2017 Fundamentals of Ionizing Radiation Dosimetry. (New York: Wiley)
```

Battistoni G et al 2015 Overview of the FLUKA code Ann. Nucl. Energy 82 10-8

Bortfeld T 1997 An analytical approximation of the Bragg curve for therapeutic proton beams Med. Phys. 24 2024–33

Bourque A E, Carrier J F and Bouchard H 2014 A stoichiometric calibration method for dual energy computed tomography *Phys. Med. Biol.* **59** 2059–88

Branco D, Taylor P, Zhang X, Li H, Guindani M and Followill D 2017 An Anthropomorphic head and neck quality assurance phantom for credentialing of intensity-modulated proton therapy *Int. J. Part. Ther.* 4 40–7

Carlino A, Gouldstone C, Kragl G, Traneus E, Marrale M, Vatnitsky S, Stock M and Palmans H 2018 End-to-end tests using alanine dosimetry in scanned proton beams *Phys. Med. Biol.* 63 055001

CIRS 2020 Computerized Imaging Reference Systems Inc. CIRS Tissue Equivalent Materials TE DS Draft 062920 Computerized Imaging Reference Systems Inc. TEM-DS-062320.pdf (meditron.ch)

Clark C H, Aird E G, Bolton S, Miles E A, Nisbet A, Snaith J A D, Thomas R A S, Venables K and Thwaites D I 2015 Radiotherapy dosimetry audit: three decades of improving standards and accuracy in UK clinical practice and trials *Br. J. Radiol.* 88 20150251

Constantinou C 1978 Tissue substitutes for particulate radiations and their use in radiation dosimetry and radiotherapy Queen Mary University of London http://qmro.qmul.ac.uk/xmlui/handle/123456789/1718

Cook H, Lambert J, Thomas R, Palmans H, Hussein M, Clark C H, Royle G, Pettingell J and Lourenço A 2022 Development of a heterogeneous phantom to measure range in clinical proton therapy beams *Phys. Med.* **93** 59–68

Crellin A 2018 The road map for national health service proton beam therapy *Clin. Oncol.* 30 277–9

Farr J B et al 2021 Clinical commissioning of intensity-modulated proton therapy systems: report of AAPM Task Group 185 Med. Phys. 48 e1–30 Ferrari A and Sala P R 1993 A new model for hadronic interactions at intermediate energies for FLUKA code Presented at the Int. Conf. on Monte Carlo Simulation in High Energy and Nuclear Physics, Tallahassee (Florida)

Goma C, Almeida I P and Verhaegen F 2018 Revisiting the single-energy CT calibration for proton therapy treatment planning: a critical look at the stoichiometric method *Phys. Med. Biol.* 63 235011

Gottschalk B 2010 On the scattering power of radiotherapy protons Med. Phys. 37 352-67

Grant R L, Summers P A, Neihart J L, Blatnica A P, Sahoo N, Gillin M T, Followill D S and Ibbott G S 2014 Relative stopping power measurements to aid in the design of anthropomorphic phantoms for proton radiotherapy J. Appl. Clin. Med. Phys 15 121–6

Griffith R V, Anderson A L and Dean P N 1976 Further realistic torso phantom development UCRL-50007-76-1Lawrence Livermore Laboratory, Livermore, CA

ICRU 44 1993 Tissue substitutes in radiation dosimetry and measurement report44International Commission on Radiation Units and Measurements ICRU 63 2000 Nuclear Data for Neutron and Proton Radiotherapy and for Radiation Protection63International Commission on Radiation Units and Measurements

Leeds Test Object 2014 Tissue Equivalent Materials: The Original Tissue Equivalents Leeds Test Objects Doc 363c Tissue Equivalent Materials_specSheet.cdr (leedstestobjects.com)

Lewis D J, Taylor P A, Followill D S, Sahoo N, Mahajan A, Stingo F C and Kry S F 2018 A new anthropomorphic pediatric spine phantom for proton therapy clinical trial credentialing *Int. J. Part. Ther.* 4 20–7

Lourenço A et al 2017 Evaluation of the water-equivalence of plastic materials in low- and high-energy clinical proton beams *Phys. Med. Biol.* 62 3883–901

Lourenço A, Thomas R, Bouchard H, Kacperek A, Vondracek V, Royle G and Palmans H 2016 Experimental and Monte Carlo studies of fluence corrections for graphite calorimetry in low- and high-energy clinical proton beams *Med. Phys.* 43 4122–32

Newhauser W D and Zhang R 2015 The physics of proton therapy Phys. Med. Biol. 80 155–209

Paganetti H 2017 Proton Beam Therapy. (Bristol: IOP Publishing) 2399-891

Palmans H et al 2013 Fluence correction factors for graphite calorimetry in a low-energy clinical proton beam: I. Analytical and Monte Carlo simulations *Phys. Med. Biol.* 58 3481–99

Palmans H, Symons J E, Denis J M, De Kock E A, Jones D T L and Vynckier S 2002 Fluence correction factors in plastic phantoms for clinical proton beams *Phys. Med. Biol.* 47 3055–71

Rasouli F S, Masoudi S F and Jette D 2016 Technical Note: On the analytical proton dose evaluation in compounds and mixtures *Med. Phys.* 43 303–7

Schneider U, Pedroni E and Lomax A 1996 The calibration of CT Hounsfield units for radiotherapy treatment planning *Phys. Med. Biol.* 41

Snyder W S, Cook M J, Nasset E S, Karhausen L R, Howells G P and Tipton I H 1975 Report on the Task Group on Reference

Man23International Commission of Radiological Protection P023 Report on the Task Group on Reference Man (sagepub.com)

Stacey A J, Bevan A R and Dickens CW 1961 A new phantom material employing depoymerised natural rubber Br. J. Radiol. 34 510–5 Sun Nuclear 2019 Advanced Electron Density Phantom (GammexTM Technology) - Sun Nuclear

Taylor P A, Lowenstein J, Followill D and Kry S F 2022 The value of on-site proton audits *Int. J. Radiat. Oncol. Biol. Phys.* 112 1004–11

Thomas R A S, Bolt M A, Bass G, Nutbrown R, Chen T, Nisbet A and Clark C H 2017 Radiotherapy reference dose audit in the United Kingdom by the National Physical Laboratory: 20 years of consistency and improvements *Phys. Imaging Radiat. Oncol.* 3 21–7

Vlachoudis V 2009 Flair: A powerful but user friendly graphical interface for FLUKA Proc. Int. Conf. on Mathematics, Computational Methods & Reactor Physics (M&C 2009), Saratoga Springs, New York

White D 1978 Tissue substitutes in experimental radiation physics *Phys. Med. Biol.* 5 467–79

White DR 1974 The formulation of substitute materials with predetermined characteristics of radiation absorption and scattering Queen Mary University of London http://qmro.qmul.ac.uk/xmlui/handle/123456789/28511

White DR 1977 The formulation of tissue substitute materials using basic interaction data *Phys. Med. Biol.* 22 889–99

White DR, Martin RJ and Darlison R 1977 Epoxy resin based tissue substitutes Br. J. Radiol. 50 814-21

Woodard H Q and White D R 1986 The composition of body tissues Br. J. Radiol. 64 149-59

Xu X G and Eckerman K 2009 Handbook of Anatomical Models for Radiation Dosimetry. (Boca Raton, FL: CRC Press)

Zhang R and Newhauser W D 2009 Calculation of water equivalent thickness of materials of arbitrary density, elemental composition and thickness in proton beam irradiation *Phys. Med. Biol.* **54** 1–19